Experimental Evaluation of an IR and US Multi-Sensory Positioning Fusion Method

Elena Aparicio-Esteve[1], José M. Villadangos[1], Álvaro Hernández[1] and Jesús Ureña[1]

[1]*Electronics Department, University of Alcala, Alcalá de Henares (Madrid), Spain*

Abstract

Certain indoor applications, mainly related to unmanned mobile vehicles or accurate monitoring of targets, robots or people, require positioning systems with centimeter accuracy. Although some RF-based systems, such as UWB, have recently provided commercially available solutions for that purpose, ultrasound- or infrared-based systems still represent a feasible approach, due to their particular features and advantages. Whether having a direct line of sight between the emitting beacons and the receivers, these systems provide signal confinement in a reduced environment (typically room level), thus providing high robustness against external interference. Furthermore, their combination in mixed solutions may also achieve better performances, by mitigating the complementary drawbacks from each other, covering larger areas while minimizing interferences between beacons (alternating technologies), or increasing the availability of measurements. In this context, this work describes the experimental evaluation of a loosely-coupled fusion method that merges two positioning systems, one based on ultrasounds and the other on infrareds. Both systems are described hereinafter, and the range and accuracy performance individually obtained are presented as well. Experimental results for both systems are similar in terms of accuracy (below 15 cm between 80 and 95% of cases) in the common coverage area. These figures are similar when measurements are merged by means of a Kalman Filter (KF) into a single position estimate, while increasing the availability of the final system and discarding the effect from possible outliers in the original independent estimates.

Keywords

Local Positioning System (LPS), Ultrasound, Infrared, Kalman Filter

1. Introduction

Some positioning applications and services only requires a contextual location (room level), such as guiding/monitoring people or customized advertising on mobile devices in commercial centres. Nevertheless, in other cases the accuracy and availability in the determination of a target's position become a challenging issue, where only errors in the range of decimetres or centimetres are accepted, in unmanned vehicle guidance for example. Furthermore, there are other features that are also desirable in a local positioning system (LPS): the ease of deployment and derived costs, the coverage, the compatibility with other exiting systems (including communications), privacy policy, or the robustness against external interference. In general terms, positioning

IPIN 2021 WiP Proceedings, November 29 – December 2, 2021, Lloret de Mar, Spain

elena.aparicio@uah.es (E. Aparicio-Esteve); jm.villadangos@uah.es (J. M. Villadangos); alvaro.hernandez@uah.es (Á. Hernández); jesus.urena@uah.es (J. Ureña)

0000-0001-7886-312X (E. Aparicio-Esteve); 0000-0001-5900-0978 (J. M. Villadangos); 0000-0001-9308-8133 (Á. Hernández); 0000-0003-1408-6039 (J. Ureña)

systems can be classified according to the sensory technology involved [1]: optical, mechanical, magnetic, acoustic, or radio frequency (RF).

On the other hand, the widespread use of mobile devices, such as smartphones or tablets, with connection to Internet anywhere and anytime, has emerged a huge variety of location-based services and applications using location, taking advantage of the communication nodes already deployed. This approach is commonly based on the existing infrastructures (WiFi nodes, for example), or on ad-hoc networks (such as Bluetooth Low Energy) [2, 3], but with a clear predominance of radio-frequency technologies. A particular interesting proposal, with high accuracies (lower than decimetres), is ultra-wide band (UWB), which has emerged as a suitable solution for indoor positioning, and it has already begun to be integrated into advanced versions of smartphones. Another positive aspect of UWB is its large coverage and range capabilities (more than 100 m in direct Line-Of-Sight, LOS). Furthermore, UWB transmissions can partially penetrate walls and obstacles, although their accuracy and maximum range are greatly reduced in practice when operating indoors, especially due to the NLOS (Non-Line-Of-Sight) effect and the influence from the environment [4]. UWB-based systems are likely to keep improving themselves and decreasing their price, so they will play a predominant role in most indoor positioning applications in coming years. However, it is also worldwide accepted that different technologies may be complementary for indoor positioning in many cases, depending on the application under study.

With regard to ultrasound-based LPS [5, 6], they usually provide a low cost whereas errors are in the range of centimeters, being necessary to deal with some drawbacks, such as multipath or near-far effects. The most typical arrangement in ultrasonic LPSs is the deployment of fixed transmitting beacons at known positions [7, 8], so those receiving targets in the coverage area can detect the corresponding transmissions and determine the Times-of-Arrival (ToA) or the Time-Differences-of-Arrival (TDoA) to estimate their own positions by means of spherical or hyperbolic trilateration, respectively [9].

Concerning infrared-based LPSs, there is an emerging interest nowadays in this optical technology, thanks to all the LED lamps already existing in public buildings, companies and homes. This implies likely a low cost, as well as broad distribution in the vast majority of indoor spaces [10, 11]. Infrared Local Positioning Systems (IRLPS) commonly apply triangulation for positioning estimation, as they consist of measuring the Angles-of-Arrival (AoA). This approach avoids, not only involving the velocity of light in calculations when using Times-of-Flight (ToF), but also the influence from light reflections and the multipath effect [12].

In this context, this work evaluates a loosely-coupled fusion method to merge two different LPS, based on optical and ultrasonic technologies, which cover a common area and whose measurements can be acquired simultaneously. Merging both systems enhances the coverage area with a higher reliability and availability. The position estimates coming from both are fused by means of a Kalman filter (KF) to provide a more robust estimated position. The whole proposal has been validated experimentally, achieving the final approach positioning errors in the range of 10 cm for almost 90% of cases. The rest of the manuscript is organised as follows: Sections II and III describe the infrared and ultrasonic LPSs, respectively; Section IV presents the obtained experimental results; and, finally, conclusions are discussed in Section V.

2. Description of the Infrared LPS

The infrared LPS is based on a set of four emitters or LED beacons placed at known positions, so that they cover a certain area where the receiver can estimate its position. A general scheme of the proposal is presented in Fig. 1. It is assumed hereinafter that the LEDs are placed in the ceiling, whereas the receiver can move in a certain plane (for example, on the ground). The transmitters are neither rotated nor inclined, while the receiver can be rotated in the Z axis. Thus, the proposed system can be applied in its current configuration as a 3D IRLPS to obtain the pose of a mobile robot (x, y, z, γ), even when a low SNR (Signal-to-Noise Ratio) is expected (distances even greater than about 4 meters with 0.5 W emitters).

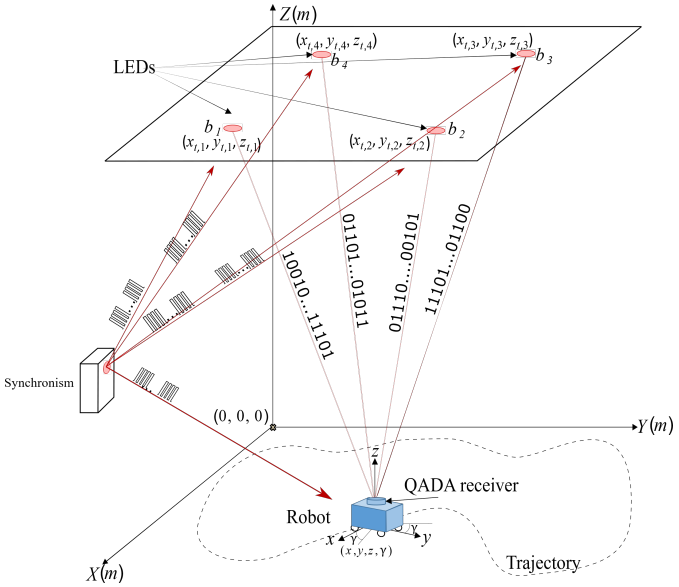

Figure 1: Proposed infrared-based LPS.

Every LED transmits an 1151-bit LS sequence c_i with a BPSK (Binary Phase Shift Keying) modulation with a carrier of 25 kHz [13]. The reception system consists of a QADA (Quadrant photodiode Angular Diversity Aperture) circular photoreceptor QP50-6-18u-TO8 [14], a filtering stage, a synchronism detector and an acquisition system STM32F469I Discovery [15] connected by USB to a computer, where the detected signals are processed. The light emitted by the LEDs illuminates the QADA receiver, thus generating four currents (one per quadrant). The QADA receiver actually provides three output currents: the sum of all quadrant currents (v_{sum}), and the differences of currents in the axes X (v_{lr}) and Y (v_{bt}). These three signals are acquired and processed to obtain the point of incidence (x_r, y_r) of the transmitters on the surface of the QADA.

It is worth noting that emitters and receivers are synchronized by means of an additional infrared synchronism beacon. It emits a pulse every 2 Hz and, when the receiver module detects it, it begins to acquire simultaneously with the emitters' transmission. A CDMA (Code-Division Multiple Access) medium access technique has been considered, where each transmission is identified by using a matched filter for every transmitted code. This procedure is based on the

correlation of the received signals v_{sum}, v_{lr} and v_{bt} with the transmitted codes c_i, while reducing other interference (noise, ambient light, incident sunlight, etc.). The resulting correlation peaks allow to obtain the ratios (p_x, p_y) between the correlation peaks of the difference signals and the correlation peak of the sum signal. Afterwards, the position of the image point projected on the QADA photoreceptor can be estimated for each transmitter according to (1). Note that the misalignment of the aperture δ has also been considered as an intrinsic parameter when estimating the image points (x_r, y_r), as well as its central point (x_c, y_c), the aperture length l and the ratio between the expected focal length hap and the actual focal length h'_{ap}: $\lambda = h'_{ap}/h_{ap}$.

$$\begin{bmatrix} x_r \\ y_r \end{bmatrix} = \frac{-l}{2} \cdot \lambda \cdot \begin{bmatrix} p_x + \delta \cdot p_y \\ -\delta \cdot p_x + p_y \end{bmatrix} + \begin{bmatrix} x_c \\ y_c \end{bmatrix} \tag{1}$$

After estimating the positions of the image points (x_r, y_r) for each emitter i, the algorithm detects the rotation γ of the receiver around the Z axis. Since the transmitters are arranged in a square, the image points must have the same shape. Therefore, if the receiver rotates a certain angle γ around the Z axis, the image points will also rotate an angle γ. The rotation angle γ is obtained by means of trigonometric equations using the rotated image points (x_r, y_r) [13], and then the image points can be unrotated. This step is necessary as the final positioning algorithm requires the receiver to be aligned with the reference frame. The positioning algorithm continues with the estimation of the final coordinates (x, y, z) of the receiver by using an LSE (Least Squares Estimator), as well as different trigonometric considerations [16].

To detail how the proposed IRLPS behaves in the test area, the Position Dilution of Precision (PDOP) is presented in Fig. 2 when the receiver is located at a height of $z = 0$ m (on the floor). The projection of the transmitters in the XY plane are also presented with black crosses. It can be clearly observed an increase of the PDOP at the corners of the coverage area, with respect to the centre of the room.

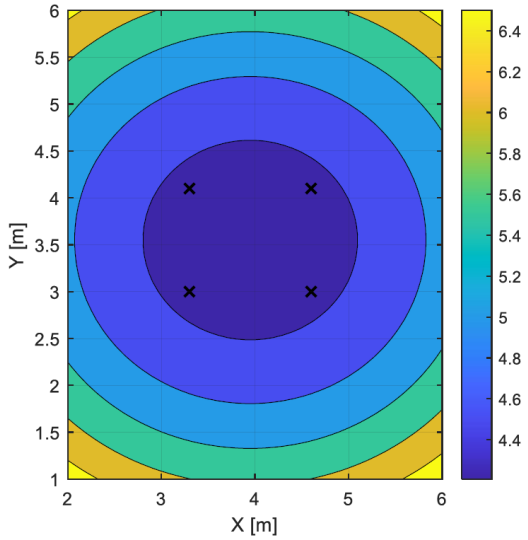

Figure 2: PDOP of the proposed IRLPS system in the coverage area for $z = 0$ m (on the floor).

3. Description of the Ultrasonic LPS

The ultrasonic LPS consists of a set of emitting beacons, together with a synchronism block. Every beacon transmits a different Kasami code with a length of 255 bits, also BPSK modulated with a carrier of 41.667 kHz [8]. Note that the modulation symbol consists of two carrier periods. The ultrasonic receiver includes a MEMS microphone SPU0414HR5H-SB [17], connected to an analog input of the STM32F103 microcontroller to acquire the incoming signal at $f_s = 100$ kHz with 8 bits. All these elements, both ultrasonic beacons and receiver, are synchronized through an IR synchronism block, based on the LPC1768 microcontroller. The synchronism beacon is the same one from the previous IRLPS, so that both positioning systems (US and IR) emit and receive simultaneously. Fig. 3 shows a general scheme of the proposed ultrasonic LPS.

To estimate the receiver's position based on the distances measured by the ToFs, the trilateration equation system is solved using the Gauss-Newton algorithm. This is an iterative approach for solving the system of non-linear equations resulting from the distance measurements derived from the ToFs between the receiver and the beacons. As before, these distances are determined again from the matched filtering between the received signal and the emitted Kasami codes. In spherical trilateration, with the location of the beacons in the plane of the ceiling, only three correct measurements are needed to estimate the receiver's position. Whether more measurements are available, the algorithm dynamically adapts and solves an oversized system. More details can be found in [8], where the ultrasonic LPS with large coverage is described, as well in [4], where the IR is added and a comparison with an UWB solution is provided.

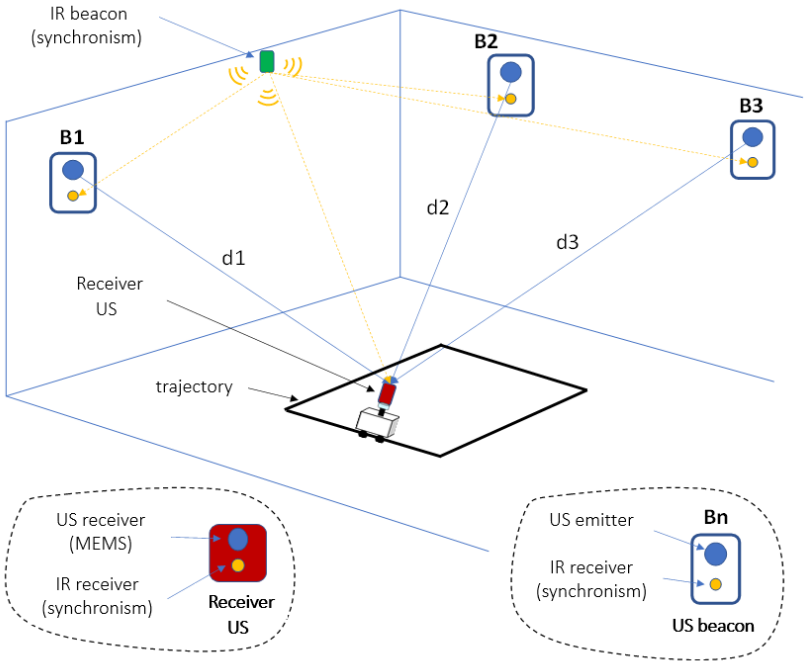

Figure 3: Proposed ultrasonic LPS.

Similar to the analysis performed for the IRLPS system, the PDOP of the proposed ULPS system is presented in Fig. 4, when the receiver is located at $z = 0$ m (on the floor). A lower PDOP is observed in the ULPS system with respect to the IRLPS system. Note that the projections of the US beacons in the XY plane are not plotted since they are located at the corners of the room, far from the central coverage area shown in Fig. 4.

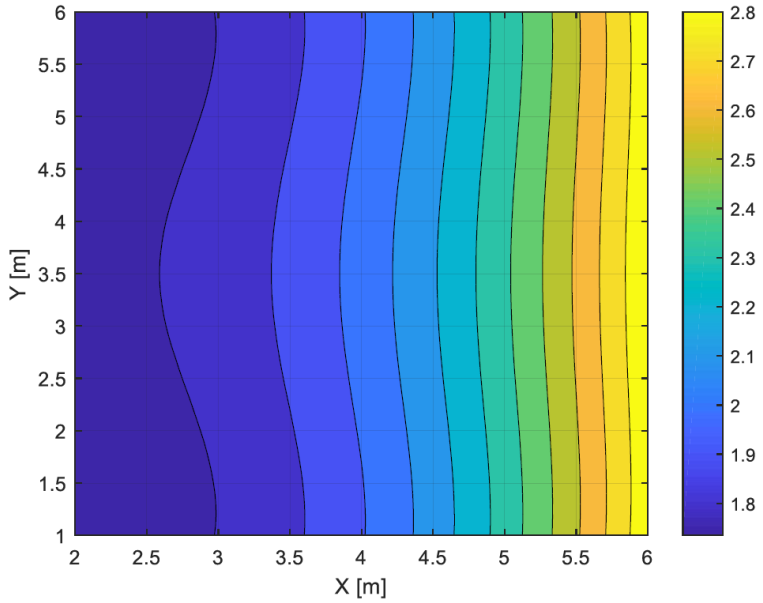

Figure 4: PDOP of the proposed ULPS system in the coverage area for $z = 0$ m (on the floor).

4. Experimental Results

The experimental tests have been carried out in a room of 8×7 m^2 with a height of 3.4 m, under normal light and noise conditions, although due to the coverage restrictions of the IR beacons, only the central part of the room has been used. The IR beacons have been placed on the ceiling of the room, in its central part, distributed at the four corners of a square with a 1.2 m long side. On the other hand, the ultrasonic beacons are at the corners of the room. The infrared (IR) and ultrasound (US) receivers are placed on a line-following robot on the room floor, as shown in Fig. 5. The ground-truth of the analysed trajectories is determined by using a Leica TS60 total station and a 360º mini prism. This is a high-precision system, which allows the 3D position of the desired object to be obtained with an accuracy of 1.5 mm.

Two trajectories are analyzed: the first one is a square with a side of 3 m (outer trajectory), whereas the second is a trajectory in an area of 2×2 m^2 (inner trajectory). Figs. 6 and 7 show the experimental measurements obtained in the XY plane using either IR or US measurements, as well as using a KF that merges both IR and US measurements. The ground-truth of the two trajectories is also plotted in a black line, and the projections of the IR and US beacons are presented with a triangle and a square, respectively. The average speed of the mobile robot

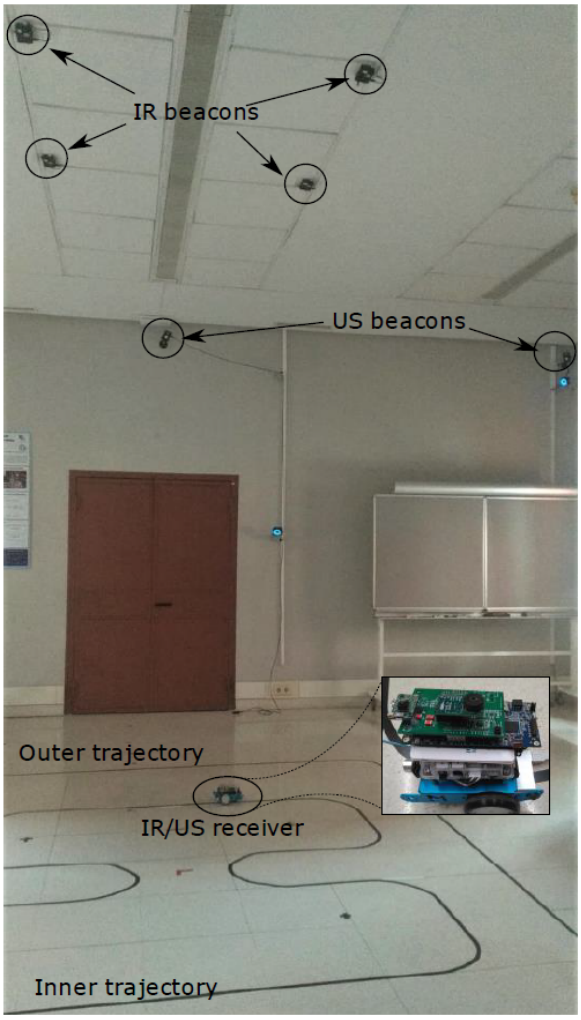

Figure 5: Experimental validation scenario for the proposed positioning systems.

during the experimental tests is 15 cm/s. Note that since the length of the IR and US signals are 46.3 ms and 12.24 ms, respectively, no great influence is associated with the speed of the robot in the acquisition of the transmitted signals.

The first step in the proposed Kalman Filter (KF) is to detect if the estimated receiver's position using the IRLPS or the ULPS is an outlier. It is considered an outlier when the difference between the position of the receiver and the previous KF solution is higher than a certain threshold. In this case, that value is neglected, and it will not enter in the KF. In particular, a threshold of 35 cm is selected. On the other hand, if both measurements are outliers, the average of the previous four KF solutions is considered as the initial estimation for the KF. Note that, this is a particular situation that only occurs in the 6.37% and 0.82% of the total measurements for the outer and the inner trajectory, respectively. This method assures that the criteria for discarding an outlier is equal for both systems.

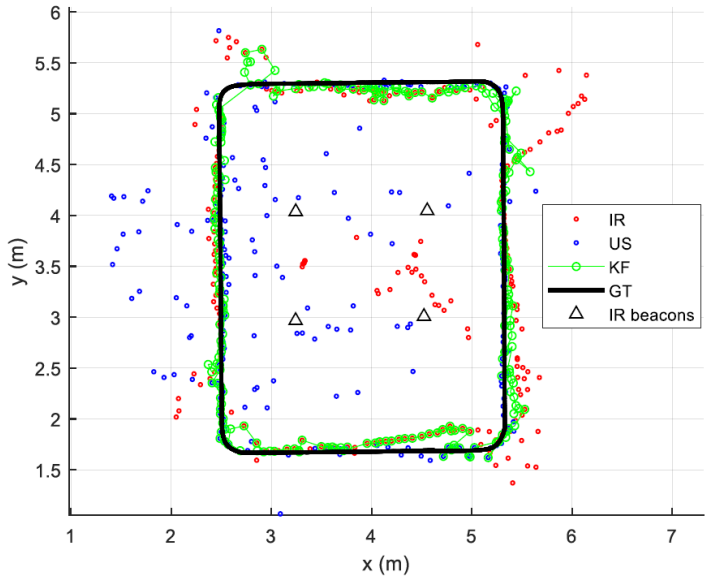

Figure 6: Estimated positions for the outer trajectory with IR and US measurements, as well as the merged solution from the KF.

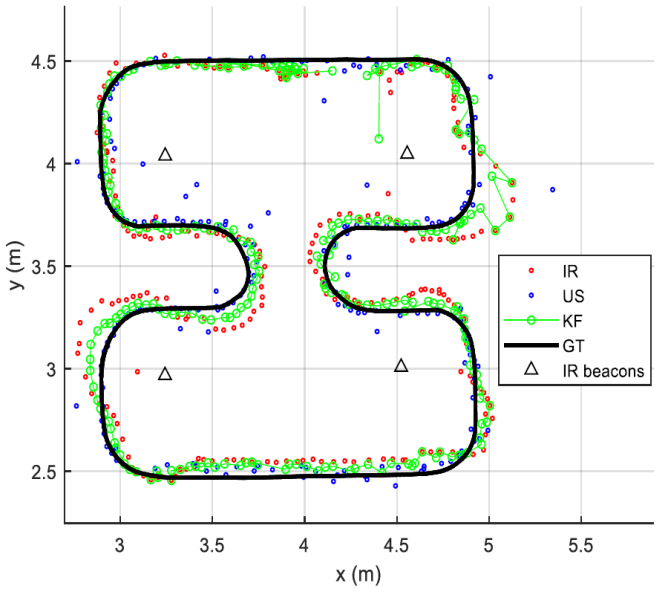

Figure 7: Estimated positions for the inner trajectory with IR and US measurements, as well as the merged solution from the KF.

The estimated coordinates x and y are plotted for both trajectories in Figs. 8 and 9, respectively, for the estimated position using the ULPS and the IRLPS, as well as the merged solution from the KF. It can be verified that the estimated position using the KF decreases the number of outliers and increases the availability of the total system.

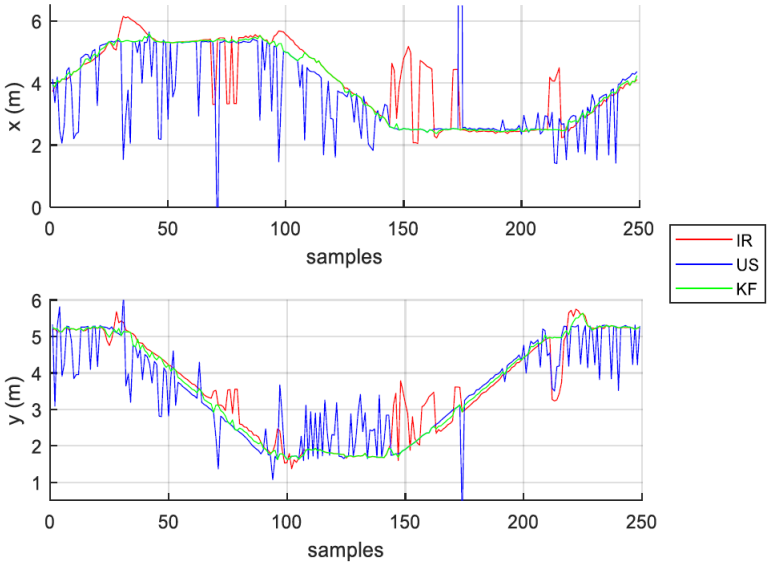

Figure 8: Estimated (x, y) positions for the outer trajectory with IR and US measurements, as well as the merged solution from the KF.

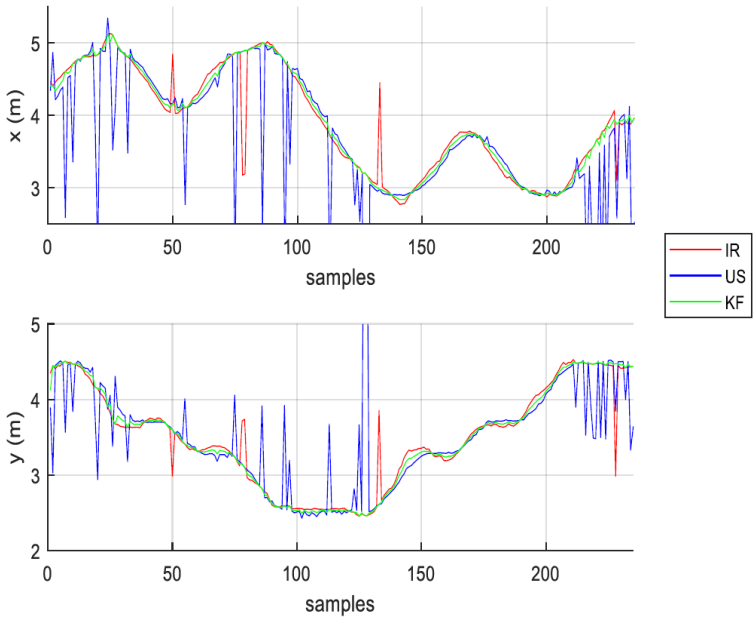

Figure 9: Estimated (x, y) positions for the inner trajectory with IR and US measurements, as well as the merged solution from the KF.

Finally, Figs. 10 and 11 show the Cumulative Distribution Functions (CDFs) of the absolute errors obtained in the XY plane for the position estimation, considering both positioning systems for the outer and the inner trajectories, respectively, as well as their mean absolute error. The

absolute error has been determined as the distance between each estimated point and the nearest ground-truth point [18]. In particular, the mean absolute errors for the IR, US and KF estimated positions are 0.24 m, 0.36 m and 0.06 m; and 0.06 m, 0.18 m and 0.03 m for the outer and inner trajectories, respectively.

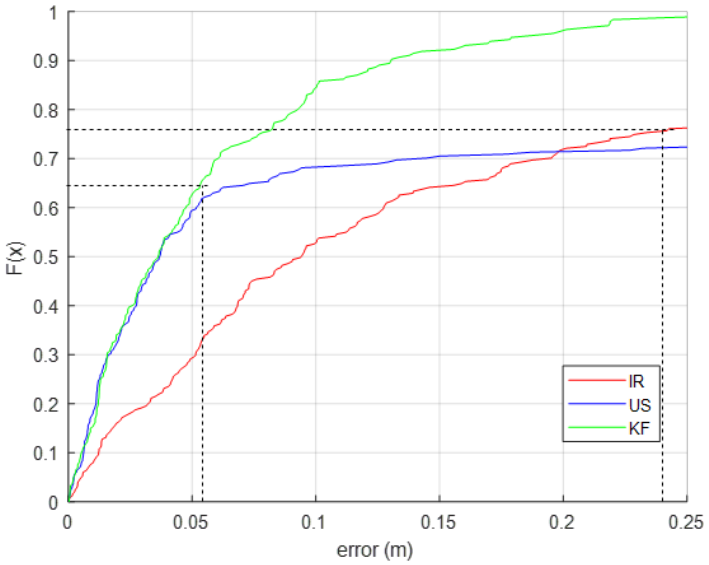

Figure 10: CDF of the absolute positioning errors for IR, US and KF measurements in the outer trajectory.

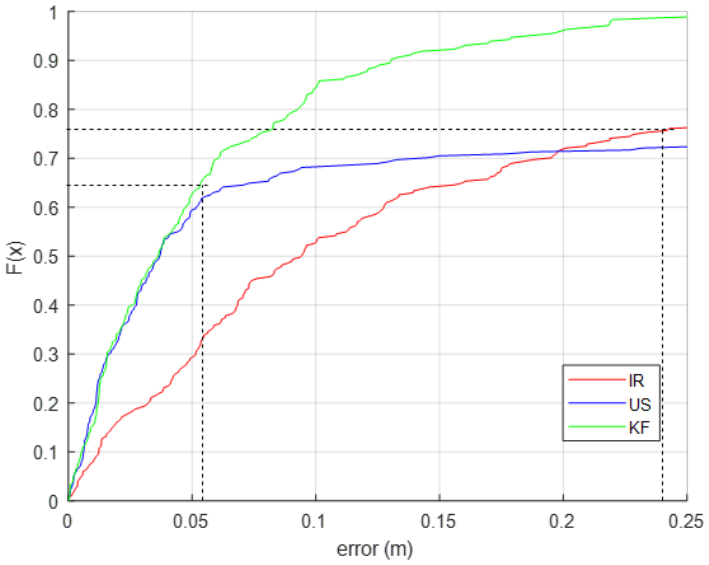

Figure 11: CDF of the absolute positioning errors for IR, US and KF measurements in the inner trajectory.

The absolute errors obtained in 90% of the cases for the KF approach are lower than 13 cm and 7 cm in the outer and inner trajectories, respectively. It can also be observed that higher errors are obtained at the corners of the room for the IR system, where there is a longer distance between the transmitters and the receiver. Both systems have errors in the same range in the inner path, where the coverage conditions are similar (although it should be remarked that the ultrasound beacons are further away as they were installed at the corners of the room). Note that the acquisitions of the IR and US signals are simultaneous, but these measurements are not simultaneous with the ground-truth measurements from the Leica total station.

Furthermore, for both analysed trajectories, there are sections where the performance of positioning systems degrades (this is where discarded outliers accumulate). This is due to particular issues in the signals' transmission (multipath conditions, low SNR, etc.). Combining the results from both systems with the KF provides a clear improvement in terms of positioning availability along the whole trajectory. It should be noted that no integration of odometry from the mobile robot has been done at this stage, although it could also help filter or mitigate the dispersion of values along the path. Future works will study using an adaptive error covariance matrix in the measurements to match the distances or angles estimated in each step of the filter.

5. Conclusions

This work has presented a comparison based on experimental tests of two different technologies used to design indoor local positioning systems. An ultrasound-based LPS has been presented, consisting of a set of beacons and a mobile receiver. On the other hand, an infrared-based LPS has also been described, with LED-based beacons installed in the ceiling and a mobile QADA receiver. Both systems are synchronised. They have been experimentally tested in a large room ($8 \times 7 \times 3.4$ m^3), with a central test area, and comparatively validated. The infrared solution presents a greater restriction in the provided coverage, which causes the performance to be reduced earlier when moving away from the room's central area (this would be mitigated by installing a larger number of IR emitters). On the other hand, their accuracy is higher than ultrasounds in the central area, perhaps also due to the distance of the ultrasonic emitters. Overall, the position errors achieved when merging both proposals with a KF are less than 10 cm in 90% of cases, while increasing the availability of the positioning system.

Acknowledgments

This work has been funded by the Spanish Ministry of Science, Innovation and Universities (project POM, ref. PID2019-105470RA-C33, and project MICROCEBUS, ref. RTI2018-095168-BC51), Comunidad de Madrid and University of Alcala (project CODEUS, ref. CM/JIN/2019-043, and project PUILPOS, ref. CM/JIN/2019-038).

References

[1] R. Mautz, Indoor positioning technologies, Ph.D. thesis, ETH Zurich, Zurich, 2012. doi:10.3929/ethz-a-007313554.

[2] J. Torres-Sospedra, R. Montoliu, S. Trilles Oliver, O. Belmonte Fernández, J. Huerta, Comprehensive Analysis of Distance and Similarity Measures for Wi-Fi Fingerprinting Indoor Positioning Systems, Expert Systems with Applications 42 (2015) 9263–9278. doi:10.1016/j.eswa.2015.08.013.

[3] F. Aranda-Polo, J. Parades, T. A. Benítez, F. Á. Franco, Improving BLE deterministic fingerprinting by using a weighted k-NN algorithm over filtered RSSI data, in: Proc. International Conference on Indoor Positioning and Indoor Navigation (IPIN 2019), 2019, pp. 431–438.

[4] D. Gualda, J. M. Villadangos, J. Ureña, A. R. J. Ruiz, F. Seco, Á. Hernández, Indoor positioning in large environments: ultrasonic and UWB technologies, in: Proc. International Conference on Indoor Positioning and Indoor Navigation (IPIN 2019), 2019, pp. 1–8.

[5] A. Ward, A. Jones, A. Hopper, A new location technique for the active office, IEEE Personal Communications 4 (1997) 42–47. doi:10.1109/98.626982.

[6] N. B. Priyantha, A. Chakraborty, H. Balakrishnan, The cricket location-support system, in: Proc. of the 6th Ann. Int. Conf. on Mobile Computing and Networking, MobiCom '00, Association for Computing Machinery, New York, NY, USA, 2000, p. 32–43. URL: https://doi.org/10.1145/345910.345917. doi:10.1145/345910.345917.

[7] Á. Hernández, E. García, D. Gualda, J. M. Villadangos, F. Nombela, J. Ureña, FPGA-Based Architecture for Managing Ultrasonic Beacons in a Local Positioning System, IEEE Transactions on Instrumentation and Measurement 66 (2017) 1954–1964. doi:10.1109/TIM.2017.2682938.

[8] J. Ureña, Á. Hernández, J. J. García, J. M. Villadangos, M. Carmen Pérez, D. Gualda, F. J. Álvarez, T. Aguilera, Acoustic Local Positioning With Encoded Emission Beacons, Proceedings of the IEEE 106 (2018) 1042–1062. doi:10.1109/JPROC.2018.2819938.

[9] M. Deffenbaugh, J. Bellingham, H. Schmidt, The relationship between spherical and hyperbolic positioning, in: OCEANS 96 MTS/IEEE Conference Proceedings. The Coastal Ocean - Prospects for the 21st Century, volume 2, 1996, pp. 590–595 vol.2. doi:10.1109/OCEANS.1996.568293.

[10] C. Wang, L. Wang, X. Chi, S. Liu, W. Shi, J. Deng, The research of indoor positioning based on visible light communication, China Communications 12 (2015) 85–92. doi:10.1109/CC.2015.7224709.

[11] T. Q. Wang, Y. A. Sekercioglu, A. Neild, J. Armstrong, Position Accuracy of Time-of-Arrival Based Ranging Using Visible Light With Application in Indoor Localization Systems, Journal of Lightwave Technology 31 (2013) 3302–3308. doi:10.1109/JLT.2013.2281592.

[12] F. Alam, M. T. Chew, T. Wenge, G. S. Gupta, An Accurate Visible Light Positioning System Using Regenerated Fingerprint Database Based on Calibrated Propagation Model, IEEE Transactions on Instrumentation and Measurement 68 (2019) 2714–2723. doi:10.1109/TIM.2018.2870263.

[13] E. Aparicio-Esteve, Á. Hernández, J. Ureña, J. M. Villadangos, F. Ciudad, Estimation of the Polar Angle in a 3D Infrared Indoor Positioning System based on a QADA receiver, in: 2019 International Conference on Indoor Positioning and Indoor Navigation (IPIN), 2019, pp. 1–8. doi:10.1109/IPIN.2019.8911775.

[14] F. S. Inc., Series 6 Data Sheet Quad Sum and Difference Amplifier, Part Description QP50-6-18u-SD2, Product Specification (2012).

[15] STMicroelectronics, STM32F469IDiscovery, Product Specification (2015) 1–40.
[16] E. Aparicio-Esteve, Á. Hernández, J. Ureña, J. M. Villadangos, Visible Light Positioning System Based on a Quadrant Photodiode and Encoding Techniques, IEEE Transactions on Instrumentation and Measurement 69 (2020) 5589–5603. doi:10.1109/TIM.2019.2962563.
[17] L. Knowles Acoustics, Amplified "ultra-mini" sisonictm microphone specificationwith maxrf protection, Product Specification (2012).
[18] M. C. Pérez-Rubio, C. Losada-Gutiérrez, F. Espinosa, J. Macias-Guarasa, J. Tiemann, F. Eckermann, C. Wietfeld, M. Katkov, S. Huba, J. Ureña, J. M. Villadangos, D. Gualda, E. Díaz, R. Nieto, E. Santiso, P. del Portillo, M. Martínez, A realistic evaluation of indoor robot position tracking systems: The IPIN 2016 competition experience, Measurement 135 (2019) 151–162. URL: https://www.sciencedirect.com/science/article/pii/S0263224118310728. doi:https://doi.org/10.1016/j.measurement.2018.11.018.